LHCb-CONF-2011-008
April 1, 2011

First observation of the decay $\overline{B}{}^0_s \to D^0 K^{*0}$ and measurement of the ratio of branching fractions $\frac{\mathcal{B}(\overline{B}{}^0_s \to D^0 K^{*0})}{\mathcal{B}(\overline{B}{}^0 \to D^0 \rho^0)}$

The LHCb Collaboration[1]

Abstract

In a data sample corresponding to ~ 36 pb^{-1} of pp collisions at a centre-of-mass energy $\sqrt{s} = 7$ TeV, we observe for the first time the decay $\overline{B}{}^0_s \to D^0 K^{*0}$. A clear signal of 34.5 ± 6.9 events is obtained with a statistical significance over 9 standard deviations and we measure its branching fraction relative to that of $\overline{B}{}^0 \to D^0 \rho^0$: $\frac{\mathcal{B}(\overline{B}{}^0_s \to D^0 K^{*0})}{\mathcal{B}(\overline{B}{}^0 \to D^0 \rho^0)} = 1.39 \pm 0.31 \pm 0.17 \pm 0.18$, where the first uncertainty is statistical, the second systematic and the third is due to uncertainty in the hadronisation fraction f_d/f_s.

[1]Conference note prepared for Moriond QCD 2011; contact authors: Aurélien Martens, Marie-Hélène Schune.

1 Introduction

A theoretically clean extraction of the CKM unitarity triangle angle γ can be performed using time-integrated $B \to DX$ decays exploiting the interference between diagrams involving $b \to u$ and $b \to c$ transitions [1, 2, 3, 4, 5]. Among the channels that can potentially be used, one of the most promising is $B^0 \to DK^{*0}$. Although this involves the decay of a neutral B meson, the final state is self-tagging so that time-dependent analysis is not required. Also, both favoured and suppressed $B^0 \to DK^{*0}$ diagrams are colour suppressed resulting in (i) slightly smaller branching fractions for $B^0 \to DK^{*0}$ decays and (ii) enhanced interference in $B^0 \to DK^{*0}$ compared to $B^+ \to DK^+$.

The decays $\overline{B}{}^0_s \to D^0 K^{*0}$ and $\overline{B}{}^0_s \to D^{*0} K^{*0}$ potentially cause significant backgrounds to the Cabibbo-suppressed $B^0 \to D^0 K^{*0}$ decay, due to the fact that $\overline{B}{}^0_s \to D^{(*)0} K^{*0}$ are Cabibbo-allowed. As shown in Fig. 1, the suppressed $B^0 \to D^0 K^{*0}$ decay (via a $b \to u$ transition which is the origin of the sensitivity to γ) and the favoured $\overline{B}{}^0_s \to D^0 K^{*0}$ decay (via a $b \to c$ transition) are reconstructed in the same final state (*i.e.*, both produce D^0, not $\overline{D}{}^0$ mesons). Moreover, the expected size of this background is not well known, since the $\overline{B}{}^0_s \to D^{(*)0} K^{*0}$ branching fractions are not yet measured. In addition, measurement of the branching fraction of $\overline{B}{}^0_s \to D^0 K^{*0}$ is of interest as a probe of SU(3) breaking in colour suppressed $B^0 \to D^0 V^0$ decays. The detailed study of $\overline{B}{}^0_s \to D^0 K^{*0}$ is thus an important and interesting milestone towards the measurement of γ.

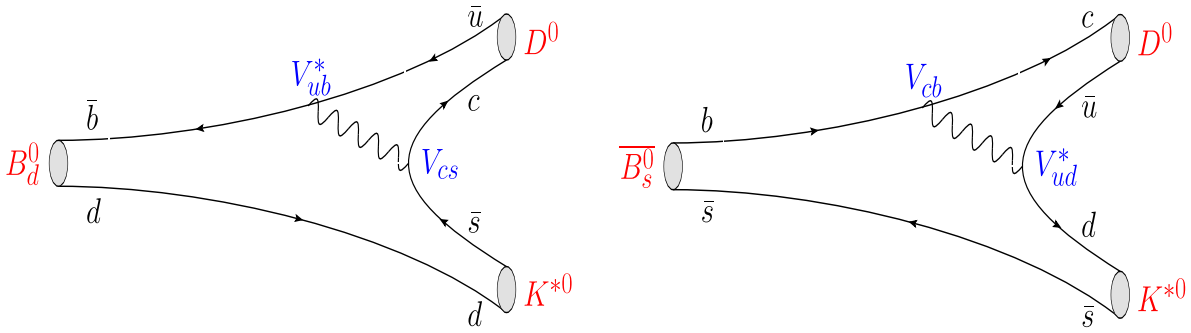

Figure 1: The main contributing diagram to the γ sensitivity is given on the left. The final state is the same as for the $\overline{B}{}^0_s \to D^0 K^{*0}$ decay that is a $b \to c$ transition, and thus enhanced compared to the $B^0 \to D^0 K^{*0}$ decay.

The strategy of the analysis is to measure a ratio of branching fractions in which most of the potentially large systematic uncertainties cancel. The decay $\overline{B}{}^0 \to D^0 \rho^0$, which has a branching fraction approximately ten times larger than $\overline{B}{}^0_s \to D^0 K^{*0}$, is used as the normalisation channel. For both numerator and denominator, the subdecay $D^0 \to K^- \pi^+$ is used. The main systematic uncertainties arise from the different particle identification requirements, and the different invariant mass and helicity angle requirements on the vector meson. Note also that the normalization of the B_s^0 decay to a B^0 decay suffers from a systematic due to uncertainty of the order of 13% in the ratio of the fragmentation

fractions $f_d/f_s = 3.71 \pm 0.47$[6].

2 The LHCb detector and dataset

The study reported here uses 36 pb^{-1} of pp collisions data collected at the Large Hadron Collider (LHC) at a centre-of-mass energy $\sqrt{s} = 7$ TeV between April and November 2010. The LHCb detector is a forward spectrometer described in detail in Ref. [7]. All detectors were fully operational and in a stable condition for the data that are included in this analysis and the vertex locator was at its closed nominal position. Fully-simulated Monte Carlo samples of signal and background events have been used to optimize the signal reconstruction and to parameterize the probability density functions (PDFs) used in the fit. Proton beam collisions are generated with `PYTHIA` and decays of hadronic particles are provided by `EvtGen` [8]. The generated particles are traced through the detector with `GEANT4`, taking into account the details of the geometry and material composition of the detector. LHCb operates a two level trigger system, a hardware trigger (L0) and a software implemented High Level Trigger (HLT). The L0 trigger reduces the visible interaction rate from 10 MHz to 1 MHz. With the HLT the trigger rate is further reduced to 2 kHz. During the data taking period of 2010, several trigger configurations were used both for the L0 and the HLT in order to cope with the varying beam conditions.

3 Selection

As mentioned above, the selection requirements are made as similar as possible for both $\overline{B}{}^0_s \to D^0 K^{*0}$ and $\overline{B}{}^0 \to D^0 \rho^0$. The cuts on the transverse momentum of the tracks (p_T), the χ^2 of the impact parameter (IP) of the track with respect to the primary vertex ($\min_{\text{PVs}} \chi^2_{\text{IP}}$) are the same in both selections. However, some differences unavoidably appear in the selection of the vector meson candidate, especially in the particle identification and mass window requirements. The tracks from the vector particles, from the D^0 and from the B^0 or B^0_s should form a vertex and cuts are applied to these vertices ($(\chi^2/\text{ndf})_{\text{vertex}}$). The K^{*0} mass window is chosen to be $\left|m^{\text{reconstructed}}_{K^{*0}} - m^{\text{PDG}}_{K^{*0}}\right| < 50$ MeV/c^2, which is the same as that used in previous studies of the $B^0 \to \overline{D}{}^0 K^{*0}$ decay [9, 10]. The mass window on the ρ^0 is also taken to be equal to the total Breit-Wigner width (± 150 MeV/c^2). The B^0 or B^0_s should point to the primary vertex: $\cos(\theta_{\text{Flight}}) > 0.99995$. The z position of the D vertex ($z_{D^0\ \text{vertex}}$) should not be situated upstream the z position of the V vertex asking for a signed significance of the distance between the two vertices to satisfy $\frac{z_{D^0\ \text{vertex}} - z_{V\ \text{vertex}}}{\sqrt{\sigma^2_{z,\ D^0\ \text{vertex}} + \sigma^2_{z,\ V\ \text{vertex}}}} > -2$ (where $\sigma_{z,\ D^0\ \text{vertex}}$ and $\sigma_{z,\ V\ \text{vertex}}$ are respectively the uncertainties on the z position of the D and V vertex). The selection thresholds are summarised in Table 1.

The particle identification requirements for both kaon and pion hypotheses have been optimized directly on data using the D^0 candidates available in the data sample. The same efficiencies are assumed for the tracks from the vector meson (both the ρ^0 and the

Particle	Variable	Threshold
$K_{K^{*0}}$	$\Delta_{K-\pi}\mathcal{L}$	> 3
	p_T	> 300 MeV/c
	$\min_{\text{PVs}} \chi^2_{\text{IP}}$	> 4
$\pi_{K^{*0}}$	$\Delta_{\pi-K}\mathcal{L}$	> -3
or π_{ρ^0}	p_T	> 300 MeV/c
	$\min_{\text{PVs}} \chi^2_{\text{IP}}$	> 4
V	$\lvert\cos\theta_{\text{Helicity}}\rvert$	> 0.4
	$\min_{\text{PVs}} \chi^2_{\text{IP}}$	> 25
	$(\chi^2/n_{\text{D.O.F.}})$ vertex	< 12
	p_T	> 1 GeV/c
K^{*0}	$\lvert m^{\text{reconstructed}}_{K^{*0}} - m^{\text{PDG}}_{K^{*0}}\rvert$	< 50 MeV/c^2
ρ^0	$\lvert m^{\text{reconstructed}}_{\rho^0} - m^{\text{PDG}}_{\rho^0}\rvert$	< 150 MeV/c^2
K_{D^0}	$\Delta_{K-\pi}\mathcal{L}$	> 0
	p_T	> 400 MeV/c
	$\min_{\text{PVs}} \chi^2_{\text{IP}}$	> 4
π_{D^0}	$\Delta_{\pi-K}\mathcal{L}$	> -4
	p_T	> 250 MeV/c
	$\min_{\text{PVs}} \chi^2_{\text{IP}}$	> 4
D^0	$(\chi^2/n_{\text{D.O.F.}})$ vertex	< 5
	$\min_{\text{PVs}} \chi^2_{\text{IP}}$	> 4
	$\lvert m^{\text{reconstructed}}_{D^0} - m^{\text{PDG}}_{D^0}\rvert$	< 20 MeV/c^2
B^0 or B^0_s	$\frac{z_{D^0\text{ vertex}} - z_{V\text{ vertex}}}{\sqrt{\sigma^2_{z,\,D^0\text{ vertex}} + \sigma^2_{z,\,V\text{ vertex}}}}$	> -2
	$\cos(\theta_{\text{Flight}})$	> 0.99995
	$(\chi^2/n_{\text{D.O.F.}})$ vertex	< 4
	$\min_{\text{PVs}} \chi^2_{\text{IP}}$	< 9

Table 1: Summary of the selection cuts used. The V particle denotes either a ρ^0 or a K^{*0}.

K^{*0}). While not fully optimal, this assumption does not lead to any bias. The thresholds are set at $\Delta_{K-\pi}\log\mathcal{L} > 0$ and $\Delta_{K-\pi}\log\mathcal{L} < 4$, respectively, for the kaon and the pion from the D^0, where $\Delta_{K-\pi}\log\mathcal{L}$ stands for the difference in logarithms of likelihoods for the K with respect to the π hypotheses. In order to keep the misidentification rate low, the thresholds for the vector meson daughters are set to $\Delta_{K-\pi}\log\mathcal{L} > 3$ and $\Delta_{K-\pi}\log\mathcal{L} < 3$. The B mass (calculated applying a mass constraint on the D^0 meson) is fitted with a double Gaussian.[2] The fit results, obtained from Monte Carlo simulation, of the B meson mass are given in Table 2. The differences due to the kinematics of the daughters of the vector mesons induce a small difference in the B mass resolution.

Multiple candidates are removed by choosing the largest flight distance significance

[2]The two Gaussian distributions have the same mean value.

Decay mode	μ	σ	κ_σ	$f_{\rm core}$
$\overline{B}{}^0_s \to D^0 K^{*0}$	5367.3 ± 0.1 MeV/c^2	10.3 ± 0.2 MeV/c^2	2.10 ± 0.06	0.82 ± 0.02
$\overline{B}{}^0 \to D^0 \rho^0$	5280.1 ± 0.1 MeV/c^2	11.2 ± 0.3 MeV/c^2	2.00 ± 0.08	0.79 ± 0.03

Table 2: B mass fit results on Monte Carlo (after all cuts). The PDF used is the sum of two Gaussian sharing the same mean μ, σ is the width of the core Gaussian, the width of the wide Gaussian is $\sigma \times \kappa_\sigma$ and $f_{\rm core}$ is the fraction of events in the core Gaussian.

among all the candidates that lie in the restricted mass windows of the D^0 and the vector meson resonance. This applies only to a small fraction of the events (of the order of 5%).

In order to extract the ratio of the branching fractions (see section 4), the data sample is divided into two categories: (i) the events which satisfy only the Hadronic L0 trigger (these events are `TOSOnly` events since they are Triggered On the Signal (TOS) exclusively and not on the rest of the event) and (ii) the events which are triggered by the rest of the event, independent of the candidate-B decay (`OtherB`). Approximately 6% of candidates do not enter either of these two categories, and are vetoed in the analysis. No specific requirement is made on the HLT.

4 Extraction of the ratio of the branching fractions

4.1 Calculation of the ratio

The ratio of the branching fractions is calculated from the number of fitted events as shown in Eq. 1, where the ϵ parameters represent the total efficiencies, including acceptance, trigger, reconstruction and selection.

$$\frac{\mathcal{B}\left(\overline{B}{}^0_s \to D^0 K^{*0}\right)}{\mathcal{B}\left(\overline{B}{}^0 \to D^0 \rho^0\right)} = \frac{N^{\rm sig.}_{\overline{B}{}^0_s \to D^0 K^{*0}}}{N^{\rm sig.}_{\overline{B}{}^0 \to D^0 \rho^0}} \frac{\mathcal{B}\left(\rho^0 \to \pi^+\pi^-\right)}{\mathcal{B}\left(K^{*0} \to K^+\pi^-\right)} \frac{f_d}{f_s} \frac{\epsilon_{\overline{B}{}^0 \to D^0\rho^0}}{\epsilon_{\overline{B}{}^0_s \to D^0 K^{*0}}} \tag{1}$$

The efficiencies of the two channels can be written as in the Eqs. 2-3. Given the fact that the selections are identical for the D^0 in the two channels of interest, the corresponding selection efficiencies cancel as well as the cuts on the topology of the decay emphasised by the $\epsilon_{B\ \rm topology}$ terms in Eqs. 2-3.

$$\epsilon_{\overline{B}{}^0 \to D^0\rho^0} = \epsilon^{\overline{B}{}^0 \to D^0\rho^0}_{\rm acceptance}\, \epsilon^{\overline{B}{}^0 \to D^0\rho^0}_{\rm reconstruction} \epsilon^{\overline{B}{}^0 \to D^0\rho^0}_{\rm trigger}\, \epsilon^{\overline{B}{}^0 \to D^0\rho^0}_{D^0\ \rm selection} \epsilon^{\overline{B}{}^0 \to D^0\rho^0}_{\rho^0\ \rm selection} \epsilon^{\overline{B}{}^0 \to D^0\rho^0}_{B\ \rm topology} \tag{2}$$

$$\epsilon_{\overline{B}{}^0_s \to D^0 K^{*0}} = \epsilon^{\overline{B}{}^0_s \to D^0 K^{*0}}_{\rm acceptance}\, \epsilon^{\overline{B}{}^0_s \to D^0 K^{*0}}_{\rm reconstruction} \epsilon^{\overline{B}{}^0_s \to D^0 K^{*0}}_{\rm trigger}\, \epsilon^{\overline{B}{}^0_s \to D^0 K^{*0}}_{D^0\ \rm selection} \epsilon^{\overline{B}{}^0_s \to D^0 K^{*0}}_{K^{*0}\ \rm selection} \epsilon^{\overline{B}{}^0_s \to D^0 K^{*0}}_{B\ \rm topology} \tag{3}$$

The ratio of the branching fractions is finally written as in Eq. 4, where the ratios of efficiencies are defined in Eqs. 5-10 and the numbers of events in the two $\overline{D}{}^0\rho^0$ trigger

categories ($N^{\texttt{TOSOnly}}_{\overline{B}^0 \to D^0\rho^0}$ and $N^{\texttt{OtherB}}_{\overline{B}^0 \to D^0\rho^0}$) are taken from data.

$$\begin{aligned}\frac{\mathcal{B}\left(\overline{B}^0_s \to D^0 K^{*0}\right)}{\mathcal{B}\left(\overline{B}^0 \to D^0\rho^0\right)} &= \frac{1}{\mathcal{B}\left(K^{*0} \to K^+\pi^-\right)}\frac{f_d}{f_s} r_{\text{acc.}} r_{\text{sel}} r_V r_{\text{PID}} r_{\texttt{OtherB}} r_{\texttt{TOSOnly}} \\ &\times \frac{N^{\text{sig.}}_{\overline{B}^0_s \to D^0 K^{*0}}}{r_{\texttt{OtherB}} N^{\texttt{TOSOnly}}_{\overline{B}^0 \to D^0\rho^0} + r_{\texttt{TOSOnly}} N^{\texttt{OtherB}}_{\overline{B}^0 \to D^0\rho^0}}\end{aligned} \tag{4}$$

$$r_{\text{acc}} = \frac{\epsilon^{\overline{B}^0 \to D^0\rho^0}_{\text{geo. acceptance}}}{\epsilon^{\overline{B}^0_s \to D^0 K^{*0}}_{\text{geo. acceptance}}} \tag{5}$$

$$r_{\text{sel}} = \frac{\epsilon^{\overline{B}^0 \to D^0\rho^0}_{\text{selection}}}{\epsilon^{\overline{B}^0_s \to D^0 K^{*0}}_{\text{selection}}} \tag{6}$$

$$r_V = \frac{\epsilon^{\overline{B}^0 \to D^0\rho^0}_{V\text{ selection}}}{\epsilon^{\overline{B}^0_s \to D^0 K^{*0}}_{V\text{ selection}}} \tag{7}$$

$$r_{\text{PID}} = \frac{\epsilon^{\overline{B}^0 \to D^0\rho^0}_{\text{PID}}}{\epsilon^{\overline{B}^0_s \to D^0 K^{*0}}_{\text{PID}}} \tag{8}$$

$$r_{\texttt{TOSOnly}} = \frac{\epsilon^{\overline{B}^0 \to D^0\rho^0}_{\texttt{TOSOnly}}}{\epsilon^{\overline{B}^0_s \to D^0 K^{*0}}_{\texttt{TOSOnly}}} \tag{9}$$

$$r_{\texttt{OtherB}} = \frac{\epsilon^{\overline{B}^0 \to D^0\rho^0}_{\texttt{OtherB}}}{\epsilon^{\overline{B}^0_s \to D^0 K^{*0}}_{\texttt{OtherB}}} \tag{10}$$

where r_{sel} is the ratio of selection efficiencies (it includes all selection cuts but the PID, the vector mass cut and the helicity cut), r_V is the ratio of efficiencies due to the vector mass cut and the helicity cut and r_{PID} is the ratio of efficiencies due to the ratio of PID efficiencies. For the trigger, the ratio of triggering efficiencies is given by $r_{\texttt{TOSOnly}}$ and $r_{\texttt{OtherB}}$.[3] The values of the r ratios are measured using simulated events except for r_{PID} which is obtained from data. Their uncertainties (quoted in Table 5) reflect the difference between data and Monte Carlo simulation.

4.2 Yields extraction

Events are assigned to distinct categories depending on the flavour of the vector resonance (K^{*0} or ρ^0). In order to simplify the description of the partially reconstructed background, the lower edge of the mass window is restricted to 5.1 GeV for the $\overline{B}^0 \to D^0\rho^0$ mode, while the lower edge of the mass window for the $\overline{B}^0_s \to D^0 K^{*0}$ mode is restricted to 5.19 GeV. Indeed, if partially reconstructed background involving D^{*0} resonances is dominant for this

[3]The values depend on the trigger configurations, they are computed from a luminosity-weighted average.

last decay mode, one expects the same background shape, shifted by the mass difference between the B_s^0 and the B^0, $\delta_\mu \approx 90\,\text{MeV}$ [11]. There are four species of events in each category: signal, combinatorial background, partially reconstructed background and cross-feed.[4] The signal PDFs for $\overline{B}^0 \to D^0\rho^0$ and $\overline{B}_s^0 \to D^0K^{*0}$ are parameterized using the sum of two Gaussians sharing the same mean value. The fraction of events in the core Gaussian as well as the ratio of the tail and core Gaussian resolutions are fixed to the values obtained from Monte Carlo simulation: $f_{\text{core}} = 0.81 \pm 0.02$ and $\kappa_\sigma = 2.04 \pm 0.05$. In order to take into account the difference in mass resolution for the $\overline{B}^0 \to D^0\rho^0$ and $\overline{B}_s^0 \to D^0K^{*0}$ decay modes the value of the ratio of widths $k_\sigma = \frac{\sigma_{D^0K^{*0}}}{\sigma_{\overline{D}^0\rho^0}} = 89 \pm 3$ % is taken from the Monte Carlo simulation and fixed to this value. Furthermore, the mass difference between the means of the B^0 and B_s^0 signals is fixed to the PDG value $\mu_{B_s^0} - \mu_{B^0} = \delta_\mu$. Only two parameters (mean and width of the B^0) are thus floated in the fit to describe the signal shapes.

The combinatorial background is described by a flat PDF, while the partially reconstructed background is parameterized by an exponential function. The exponential slope is different in the $\overline{B}^0 \to D^0\rho^0$ and $\overline{B}_s^0 \to D^0K^{*0}$ categories. Since the number of produced $\overline{B}^0 \to D^0\rho^0$ events is roughly six times larger than that of $\overline{B}_s^0 \to D^0K^{*0}$, the contribution from misidentified pions as kaons from real $\overline{B}^0 \to D^0\rho^0$ has to be taken into account. The fraction of the cross-feed signals ($f_{D^0\rho^0 \to D^0K^{*0}}$ and $f_{D^0K^{*0} \to D^0\rho^0}$) are fixed using the misidentication rates measured in data, taking also into account the difference in vector mass and helicity angle requirements using Gaussian constraints with a relative error of 50% (respectively to $f_{D^0\rho^0 \to D^0K^{*0}} = 0.062 \pm 0.031$ and $f_{D^0K^{*0} \to D^0\rho^0} = 0.095 \pm 0.047$). The PDF is parameterized by a Crystal Ball function [12, 13], whose width is fixed to 1.75 times the signal resolution, following a Monte Carlo study. Other parameters are taken from a fit to simulated events, where $\overline{B}_s^0 \to D^0K^{*0}$ is misidentified as $\overline{B}^0 \to D^0\rho^0$ or $\overline{B}^0 \to D^0\rho^0$ is misidentified as $\overline{B}_s^0 \to D^0K^{*0}$. For the $\overline{B}^0 \to D^0\rho^0$ decay mode, the events are further split according to the trigger: the `TOSOnly` and `OtherB` categories.

To summarise, the strategy is to fit simultaneously the two decay modes using an extended unbinned maximum likelihood fit of the invariant mass distributions to properly extract the yields and associated uncertainties. Four shape parameters are considered, two for signal (mean and width) and two exponential slopes for the partially reconstructed backgrounds ($c_{\text{part.},D^0\rho^0}$ and $c_{D^0\ K^{*0}}$). In addition, nine event yields are considered, three (signal, combinatorial and partially reconstructed backgrounds) in each of the three categories: $\overline{B}^0 \to D^0\rho^0$ (`TOSOnly` and `OtherB`) and $\overline{B}_s^0 \to D^0K^{*0}$. The parameters are summarized in Table 3 and Table 4.

The results of the fit for $\overline{D}^0\rho^0$ are given in Figs. 2-3. The sum over the two categories is performed only for completeness and shown in appendix A. The signals for $\overline{B}^0 \to D^0\rho^0$ are clearly visible. The overall yield is equal to 154.5 ± 14.3 signal events. The resolution of the $\overline{B}^0 \to D^0\rho^0$ mass is 14.9 ± 1.4 MeV/c^2 which is in reasonable agreement but slightly larger than the value obtained from Monte Carlo simulation. The result of the fit for the

[4] The cross-feed events are due to particle misidentification on one of the vector tracks; some $D^0\rho^0$ events can be selected as D^0K^{*0} and *vice-versa*.

Parameter	Fitted value	Comment
μ_{B^0}	5277.1 ± 1.5 MeV/c^2	free
mass difference between B^0 and B_s^0	86.8	fixed to PDG value
$f_{\rm core}$	0.81	fixed from Monte Carlo
κ_σ	2.04	fixed from Monte Carlo
$k_\sigma = \sigma_{D^0K^{*0}}/\sigma_{\overline{D}^0\rho^0}$	0.92	fixed from Monte Carlo
$\sigma_{\overline{D}^0\rho^0}$	14.9 ± 1.4 MeV/c^2	free
$c_{\mathrm{part.},D^0\rho^0}$	-24.9 ± 4.4 $(\mathrm{GeV}/c^2)^{-1}$	free
$c_{D^0\ K^{*0}}$	-17.3 ± 8.0 $(\mathrm{GeV}/c^2)^{-1}$	free
$\mu^{\rm CB}_{\overline{B}^0\to D^0\rho^0}$	5327.8 MeV/c^2	fixed from Monte Carlo
$\sigma^{\rm CB}_{\overline{B}^0\to D^0\rho^0}/\sigma_{\overline{D}^0\rho^0}$	1.75	fixed from Monte Carlo
$\alpha^{\rm CB}_{\overline{B}^0\to D^0\rho^0}$	-0.66	fixed from Monte Carlo
$n^{\rm CB}_{\overline{B}^0\to D^0\rho^0}$	3.4	fixed from Monte Carlo
$\mu^{\rm CB}_{\overline{B}^0_s\to D^0K^{*0}}$	5321.3 MeV/c^2	fixed from Monte Carlo
$\sigma^{\rm CB}_{\overline{B}^0_s\to D^0K^{*0}}/\sigma_{D^0K^{*0}}$	1.75	fixed from Monte Carlo
$\alpha^{\rm CB}_{\overline{B}^0_s\to D^0K^{*0}}$	0.59	fixed from Monte Carlo
$n^{\rm CB}_{\overline{B}^0_s\to D^0K^{*0}}$	2.3	fixed from Monte Carlo

Table 3: Summary of the fixed and fitted shape parameters with the result of the fit to real data.

$\overline{B}^0_s \to D^0K^{*0}$ is shown in Fig. 4 and the yield is equal to 34.5 ± 6.9 events.

4.3 Nonresonant contributions

In order to check the existence of other contributions below the vector mass peaks, an sPlot technique [14] has been used. The resulting plots are shown in Fig. 5. While the K^{*0} region is extremely clean, the ρ^0 region shows more complicated structure. An effective "non-ρ^0" contribution has been estimated using a second-order polynomial: 30.1 ± 7.9 events contribute in the ρ^0 mass window (± 150 MeV/c^2). The measured $\overline{B}^0 \to D^0\rho^0$ yield is corrected by this amount.

parameter	fitted value	comment
$N^{\text{comb.}}_{D^0K^{*0}}$	30.5 ± 8.8	free
$N^{\text{comb., TOSOnly}}_{\overline{D}^0\rho^0}$	95.5 ± 11.7	free
$N^{\text{comb., OtherB}}_{\overline{D}^0\rho^0}$	176.0 ± 15.5	free
$N^{\text{part.}}_{D^0K^{*0}}$	18.8 ± 11.2	free
$N^{\text{part., TOSOnly}}_{\overline{D}^0\rho^0}$	55.3 ± 8.9	free
$N^{\text{part., OtherB}}_{\overline{D}^0\rho^0}$	85.5 ± 11.2	free
$f_{D^0\rho^0\to D^0K^{*0}}$	0.019 ± 0.010	Gaussian constraint
$f_{D^0K^{*0}\to D^0\rho^0}$	0.040 ± 0.018	Gaussian constraint
$N^{\text{sig.}}_{\overline{B}^0_s\to D^0K^{*0}}$	34.5 ± 6.9	free
$N^{\text{sig., TOSOnly}}_{\overline{B}^0\to D^0\rho^0}$	77.1 ± 9.7	free
$N^{\text{sig., OtherB}}_{\overline{B}^0\to D^0\rho^0}$	77.4 ± 10.5	free

Table 4: Summary of the fitted yield and cross-feed fraction parameters with the result of the fit to real data.

5 Results

5.1 Computation of the ratio of the branching fractions

Using the measured yields of the $\overline{B}^0 \to D^0\rho^0$ signal in the two trigger categories (77.1 ± 9.7 and 77.4 ± 10.5) corrected for the "non-ρ^0" events (30.1 ± 7.9) together with the $\overline{B}^0_s \to D^0K^{*0}$ yield (34.5 ± 6.9) and using the values of the r ratios given in Table 5, one can compute the ratio of the branching ratio using Eq. 4:

$$\frac{\mathcal{B}\left(\overline{B}^0_s \to D^0K^{*0}\right)}{\mathcal{B}\left(\overline{B}^0 \to D^0\rho^0\right)} = 1.39 \pm 0.31. \tag{11}$$

5.2 Systematic uncertainties

A summary of the contributions to the systematic uncertainty is given in Table 5. The relative abundances of `TOSOnly` and `OtherB` triggered events measured from simulated signal are in good agreement with those measured from data. This agreement provides confidence in the description of the trigger in the Monte Carlo simulation. Since these relative abundances are directly measured in data, they do not enter the systematic uncertainty evaluation. However, the difference in trigger efficiency between the $\overline{B}^0 \to D^0\rho^0$ and the $\overline{B}^0_s \to D^0K^{*0}$ decay modes is taken from Monte Carlo simulation – this is considered reliable since the difference arises due to the kinematical properties of the decays which

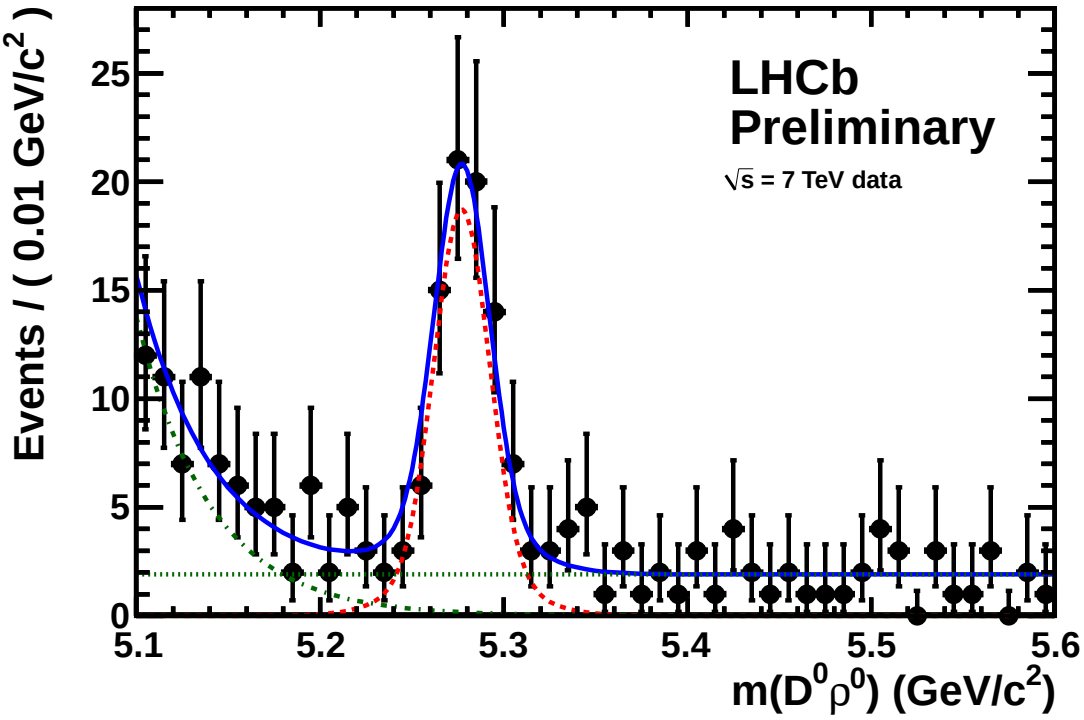

Figure 2: Invariant mass distribution for the $\overline{B}^0 \to D^0\rho^0$ decay mode for the `TOSOnly` trigger category with the fit superimposed. The black points correspond to the data and the fit result is represented as a solid blue line. The signal is fitted with a double Gaussian (dashed red line), the partially reconstructed with an exponential function (green dash-dotted line) and the combinatorial background with a flat distribution (dashed green line) as explained in the text.

are well modelled in the simulation. The difference in the energy measurement between the 2×2 first level trigger clustering and the standard 3×3 clustering is conservatively taken as a systematic uncertainty due to the hadronic trigger threshold. The systematic uncertainty due to the `OtherB` trigger performances on the two decay modes is obtained assuming that it does not depend on the decay mode ($r_{\texttt{OtherB}} = 1$).

The PID performances are determined using a data calibration sample reweighted according to the kinematical properties of our signals. The systematic uncertainty has been conservatively assigned using the results obtained without any reweighting.

The systematic uncertainty due to the PDF parametrizations has been evaluated varying the lower bound of the B invariant mass window and using alternate formulae (wide Gaussian for the partially reconstructed backgrounds, first order polynomial for the combinatorial background, single Gaussian for the signal).

The statistical uncertainty obtained on the number of "non-ρ^0" events present in the ρ^0 the mass window (± 150 MeV/c^2) has been propagated in the systematical uncertainty. The error on the ratio of the fragmentation fractions $\frac{f_d}{f_s} = 3.71 \pm 0.47$, coming from an HFAG average combining statistical and systematic uncertainties, also contributes to the

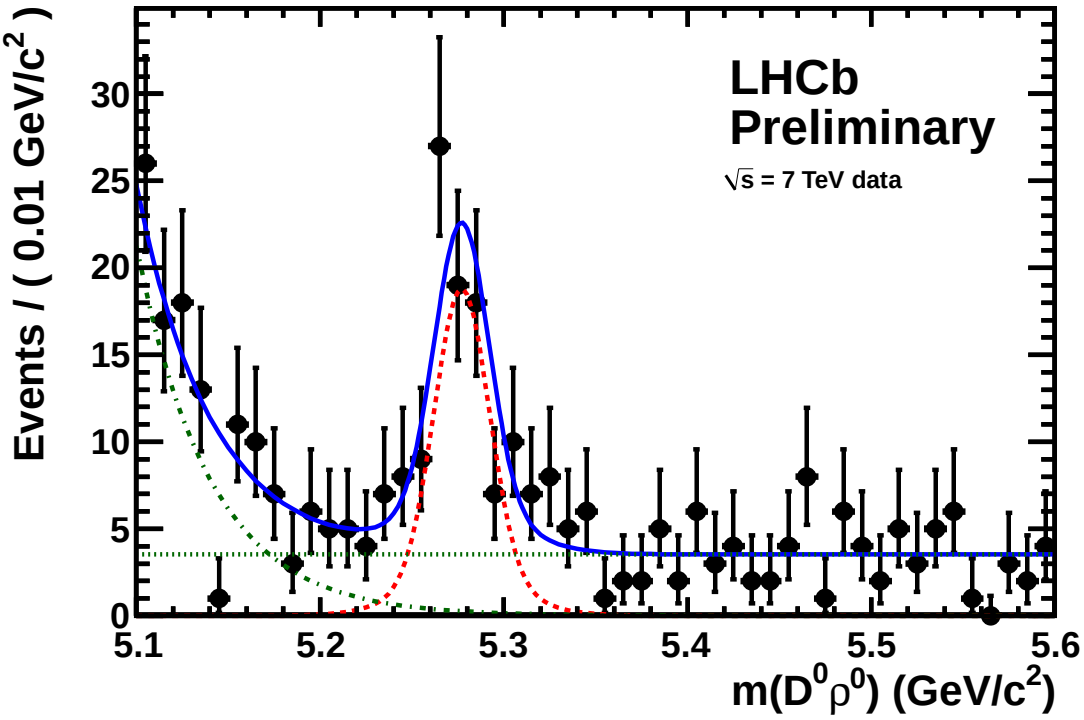

Figure 3: Invariant mass distribution for the $\overline{B}^0 \to D^0\rho^0$ decay mode for the `OtherB` trigger category with the fit superimposed. The black points correspond to the data and the fit result is represented as a solid blue line. The signal is fitted with a double Gaussian (dashed red line), the partially reconstructed with an exponential function (green dash-dotted line) and the combinatorial background with a flat distribution (dashed green line) as explained in the text.

systematic uncertainty.

6 Summary

A clear signal of 34.5 ± 6.9 $\overline{B}^0_s \to D^0 K^{*0}$ events is obtained with a statistical significance over 9 standard deviations, obtained from the change of likelihood with no signal $\overline{B}^0_s \to D^0 K^{*0}$ in the fit. The branching ratio for this decay is measured relative to that for $\overline{B}^0 \to D^0\rho^0$ to be $\frac{\mathcal{B}\left(\overline{B}^0_s \to D^0 K^{*0}\right)}{\mathcal{B}\left(\overline{B}^0 \to D^0\rho^0\right)} = 1.39 \pm 0.31 \pm 0.17 \pm 0.18$, where the first uncertainty is statistical, the second systematic and the third one is due to the hadronisation fraction (f_d/f_s). Using the PDG value [11] for the branching fraction of the decay $\overline{B}^0 \to D^0\rho^0$ $(3.2 \pm 0.5)10^{-4}$, it can be translated into a measurement of the $\overline{B}^0_s \to D^0 K^{*0}$ branching fraction: $\mathcal{B}\left(\overline{B}^0_s \to D^0 K^{*0}\right) = (4.44 \pm 1.00 \pm 0.55 \pm 0.56 \pm 0.69)\ 10^{-4}$ where the first uncertainty is statistical, the second systematic, the third one is due to the hadronisation fraction (f_d/f_s) and the last one is due to the uncertainty of the $\overline{B}^0 \to D^0\rho^0$ branching fraction. This is the first observation of the decay $\overline{B}^0_s \to D^0 K^{*0}$.

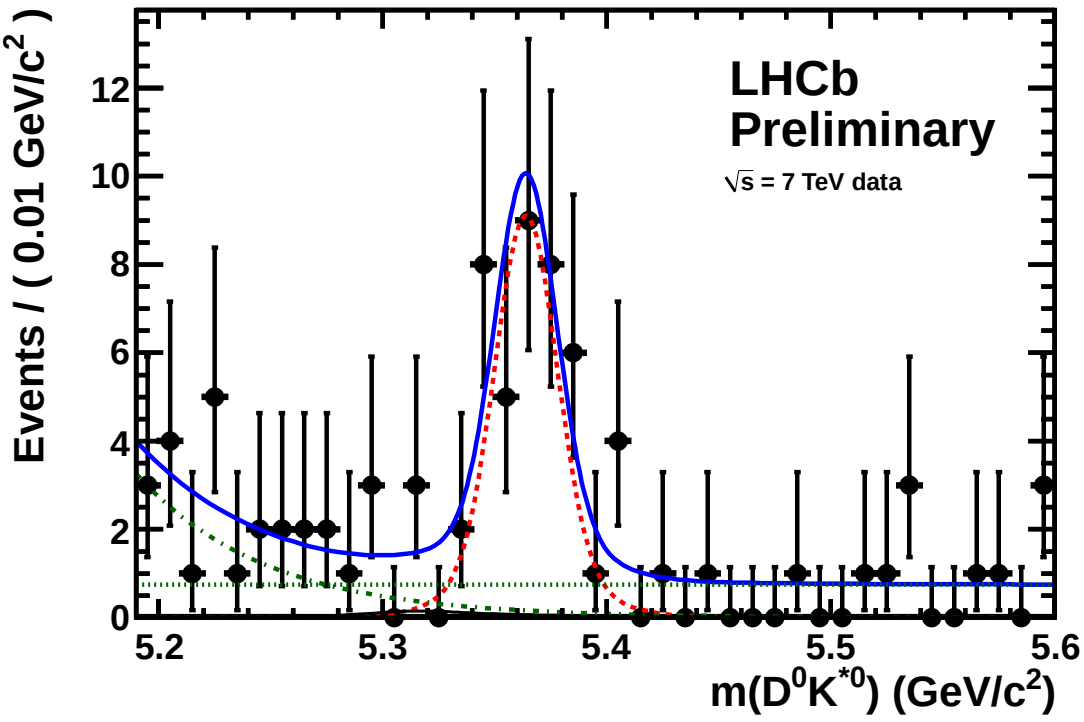

Figure 4: Invariant mass distribution for the $\overline{B}{}^0_s \to D^0 K^{*0}$ decay mode with the fit superimposed. The black points correspond to the data and the fit result is represented as a solid blue line. The signal is fitted with a double Gaussian (dashed red line), the partially reconstructed with an exponential function (green dash-dotted line) and the combinatorial background with a flat distribution (dashed green line) as explained in the text. Contributions from cross-feed are plotted in thin solid black lines.

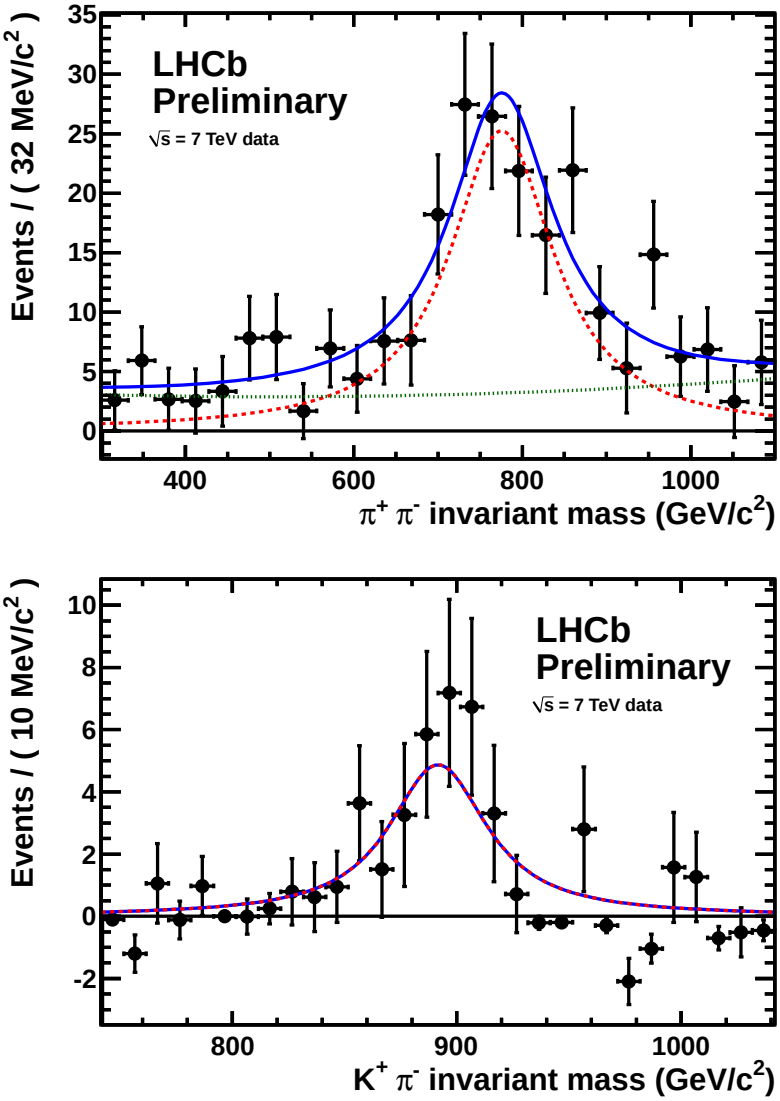

Figure 5: ρ^0 (on the top) and K^{*0} (on the bottom) invariant mass distributions obtained on data, using an sPlot technique. The level of non K^{*0} combinations in the $\overline{B}{}^0_s \to D^0 K^{*0}$ peak is clearly extremely low. The $\overline{B}{}^0 \to D^0 \rho^0$ despite being mainly due to D^0 ρ^0 combinations contains a significant contribution of "non-ρ^0" events for which one should correct. The black points correspond to the data and the fit result is represented as a solid blue line. The resonant component is fitted with a Breit-Wigner convoluted with a Gaussian (dashed red line) and the nonresonant part, if present, with a second-order polynomial (dashed green line).

Source of the uncertainty	σ_R/R, %
MC statistics $r_{\text{acceptance}} = 0.955 \pm 0.004$	0.4 %
Change in the central value of the vector mass window $r_{\text{V}} = 1.02 \pm 0.01$	1.0 %
MC statistics	1.0 %
Difference in p_T distributions of tracks between data vs MC $r_{\text{sel.}} = 0.802 \pm 0.020$	2.5 %
Use of the unweighted data calibration sample to compute $r_{\text{PID}} = 1.03 \pm 0.07$	6.8 %
L0 Hadron threshold influence on $r_{\texttt{TOSOnly}} = 1.20 \pm 0.08$	3.0 %
`OtherB` triggering efficiency independent on the mode $r_{\texttt{OtherB}} = 1.03 \pm 0.03$	1.6 %
PDF parametrizations	6.4 %
Statistical uncertainty on the " non ρ^0 " component $= 30.1 \pm 7.9$	6.8 %
Overall relative systematical uncertainty	12.3 %
HFAG average [6] for $\frac{f_d}{f_s} = 3.71 \pm 0.47$	12.7 %

Table 5: Summary of the contributions to the systematics. The uncertainty on the r ratio gives the range used for the systematic uncertainty extraction on the ratio of the branching fractions. σ_R/R stands for the resulting uncertainty on the overall correction applied to the calculation of the ratio of the branching fractions.

A Sum of the $\overline{D}^0\rho^0$ trigger categories

The plot showing the fit result for the sum of the two $\overline{D}^0\rho^0$ trigger categories is given here only for completeness. Note that only the yields from the separate categories are used for the extraction of the ratio of the branching fractions, the yields shown in Fig. 6 are not used in the analysis.

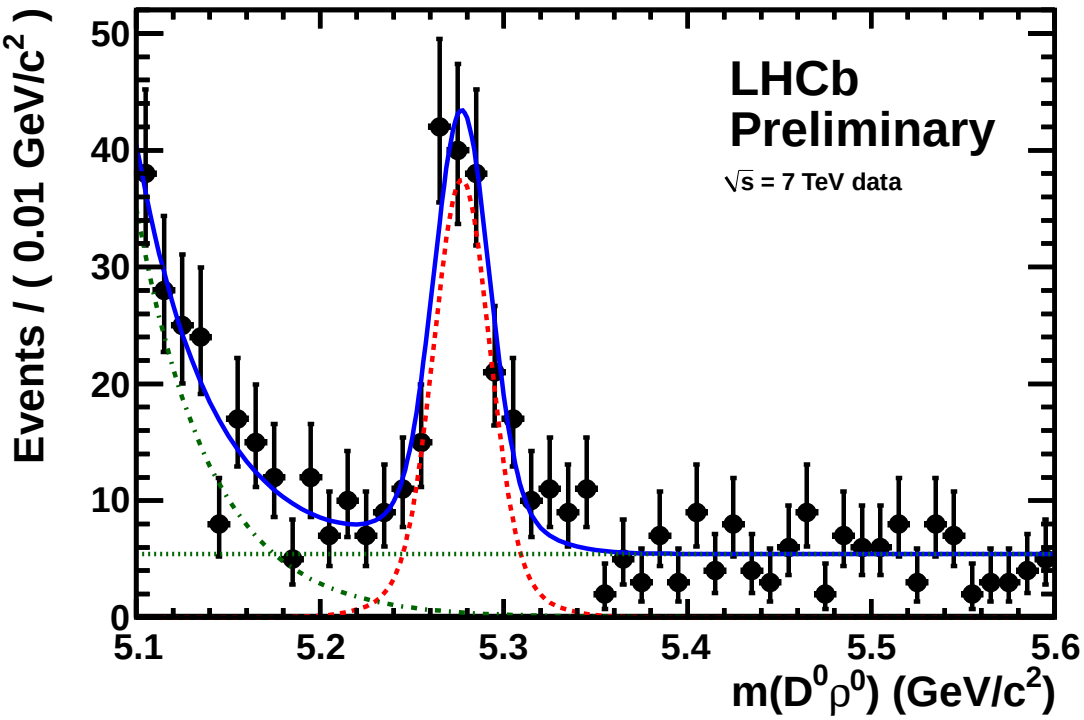

Figure 6: Shown for completeness only. Note that only the yields from Figs. 2-3 are used for the extraction of the ratio of the branching fractions. The invariant mass distribution for the $\overline{B}^0 \to D^0\rho^0$ decay mode for the sum of the two trigger categories with the fit superimposed. The black points correspond to the data and the fit result is represented as a solid blue line. The signal is fitted with a double Gaussian (dashed red line), the partially reconstructed with an exponential function (green dash-dotted line) and the combinatorial background with a flat distribution (dashed green line) as explained in the text.

References

[1] M. Gronau and D. Wyler, *On determining a weak phase from charged B decay asymmetries*, Physics Letters B **265**(1-2), 172 – 176 (1991).

[2] I. Dunietz, *CP violation with self-tagging B_d modes*, Physics Letters B **270**, 75 – 80 (1991).

[3] D. Atwood, I. Dunietz, and A. Soni, *Enhanced CP Violation with $B \to KD^0(\overline{D}^0)$ Modes and Extraction of the Cabibbo-Kobayashi-Maskawa Angle γ*, Phys. Rev. Lett. **78**(17), 3257–3260 (Apr 1997).

[4] D. Atwood, I. Dunietz, and A. Soni, *Improved methods for observing CP violation in $B \to DK$ and measuring the CKM phase γ*, Phys. Rev. D **63**(3), 036005 (Jan 2001).

[5] A. Giri, Y. Grossman, A. Soffer, and J. Zupan, *Determining γ using $B \to DK$ with multibody D decays*, Phys. Rev. D **68**(5), 054018 (Sep 2003).

[6] Heavy Flavour Averaging Group Collab., D. Asner et al., *Averages of b-hadron, c-hadron, and tau-lepton properties*.

[7] The LHCb Collaboration Collab., A.Augusto Alves et al., *The LHCb Detector at the LHC*, JINST **3**, S08005 (2008).

[8] D. J. Lange, *The EvtGen particle decay simulation package*, Nucl. Inst. Methods **A462**, 152 (2001).

[9] BABAR Collab., Bernard Aubert et al., *Measurement of $\overline{B}^0 \to D^{(*)0}\overline{K}^{(*)0}$ branching fractions*, Phys. Rev. **D74**, 031101 (2006).

[10] Belle Collab., P. Krokovny et al., *Observation of $\overline{B}^0 \to D^0\overline{K}^0$ and $\overline{B}^0 \to D^0\overline{K}^{*0}$ Decays*, Phys. Rev. Lett. **90**, 141802 (2003).

[11] Particle Data Group, K. Nakamura et al., *The Review of Particle Physics*, J. Phys. G **37**, 075021 (2010).

[12] J. Gaiser, *Charmonium spectroscopy from radiative decays of the J/ψ and ψ'*, (1982), Ph.D. Thesis.

[13] T. Skwarnicki, *A study of the radiative cascade transitions between Υ' and Υ resonances*.

[14] M. Pivk and F. R. Le Diberder, *SPlot: A Statistical tool to unfold data distributions*, Nucl.Instrum.Meth. **A555**, 356–369 (2005).